Hindawi
Shock and Vibration
Volume 2023, Article ID 2745671, 16 pages
https://doi.org/10.1155/2023/2745671

Research Article

Cross-Length of Mode Shapes in Structural Dynamics: Concept and Applications

M. Aenlle,[1] **R. Stufano**,[2] **N. García-Fernández**,[1] **F. Pelayo**,[1] **and R. Brincker**[3]

[1]*Department of Construction and Manufacturing Engineering, University of Oviedo, Gijón 33204, Spain*
[2]*Department of Civil, Environmental, Construction and Chemical Engineering, Polytechnic University of Bari, Bari, Italy*
[3]*Brincker Monitoring, Copenhagen, Denmark*

Correspondence should be addressed to N. García-Fernández; garciafnatalia@uniovi.es

Received 21 March 2023; Revised 21 April 2023; Accepted 6 May 2023; Published 29 May 2023

Academic Editor: Fabio Botta

Modal mass is one of the modal parameters that are required to define the dynamic behavior of a structure when a modal model is used. In experimental modal analysis (EMA), modal masses are the least reliable modal parameter, while in operational modal analysis (OMA), modal masses cannot be estimated because the exciting forces are not measured. In this paper, the concept of cross-length between mode shapes is formulated for continuous and discrete systems, and important properties are derived from this definition. It is demonstrated that the cross-length is zero for all modes in constant mass density systems. For structures consisting of parts with different mass density, equations that relate the partial cross-lengths over the different volumes and the total masses of the different parts can be formulated for each mode, i.e., there is a relationship between the cross-length and the total mass of the parts with different mass density. The equations proposed in the paper have been validated through numerical simulations and experimental testing on two lab-scaled structures. This methodology can also be applied as a correlation technique, specifically to determine how the mass is distributed in the structure, as well as a technique to construct a proportional FRF in constant mass density systems.

1. Introduction

When a modal model is used in structural dynamics to describe the dynamic behavior of a structure, four modal parameters are required: natural frequencies, modal masses, mode shapes, and damping ratios. In experimental modal analysis (EMA), modal mass is the least reliable parameter, and it is also highly sensitive to response magnitude.

In operational modal analysis (OMA), modal masses cannot be estimated because the forces are not measured. Therefore, several techniques for scaling mode shapes (mass normalization) have been extensively studied in recent years. According to Brandt [1], these methodologies can be divided into the following categories:

(1) Methods based on the repetition of OMA tests with several configurations of the structure (modifying its dynamic behavior). These methodologies are mainly based on changing the mass of the structure [2–5] and have been successfully validated in practical applications [2–5]. However, performing static mass modifications can be challenging in real applications, such as civil structures where large masses are required. Several methodologies have been proposed to overcome this inconvenience. In bridges, moving vehicles can be used to modify the mass of the structure [6–10], but the traffic must shut down. Sheibani et al. [11, 12] proposed to consider traffic loading as the source of mass modification.

(2) Methods based on operational modal analysis with exogenous inputs (OMAX) where the unmeasured environmental excitation is complemented with an additional measured force provided by external actuators [13–15].

(3) Methods relying on OMA tests with the use of specific dynamic systems coupled to the main structure, such as tuned-mass dampers (TMD) [16]

or by adding people to the system and using a database of pedestrian excitation [17].

(4) Methods based on using harmonic forces (OMAH). This procedure involves the use of general-purpose actuators and simple signal processing [18–20].

(5) Methods relying on finite element models [21], which combine the mass matrix or the modal masses of the numerical model with the experimental mode shapes.

The magnitude and units of the modal mass depend on the method used to normalize the mode shapes. A mode shape is considered to be mass normalized when the modal mass m is dimensionless unity, i.e., $m = 1$, while it is defined as unscaled when it is not mass normalized [22–30]. The unscaled mode shape vector $\boldsymbol{\psi}$ and the scaled (mass-normalized) mode shape vector $\boldsymbol{\phi}$ are related through the expression [5, 31]

$$\boldsymbol{\phi} = \frac{1}{\sqrt{m}}\boldsymbol{\psi}. \tag{1}$$

Besides mass normalization, normalizing to the unit length and the largest component (or to the n-th DOF component) equal to unity are the most common techniques used for mode shape normalization.

A mode shape $\boldsymbol{\psi}$ can be normalized to the unit length by means of the expression

$$\boldsymbol{\psi}_{\mathbf{L}} = \frac{\boldsymbol{\psi}}{L_{\psi}}, \tag{2}$$

where $\boldsymbol{\psi}_{\mathbf{L}}$ indicates mode shape normalized to the unit length and L_{ψ} is the length of the mode shape.

The Euclidean length L_E of a mode shape $\boldsymbol{\psi}(\mathbf{x})$ in one-dimensional continuous systems is defined as [32]

$$L_E = |\boldsymbol{\psi}| = \sqrt{\int_{\mathbf{0}}^{\mathbf{L}} |\boldsymbol{\psi}(\mathbf{x})|^2 \mathrm{d}x}, \tag{3}$$

where the subindex "E" indicates Euclidean. However, the length L_E given by equation (3) is not dimensionless, although the mode shape is.

The Euclidean length (or Euclidean norm) of a real discrete vector $\boldsymbol{\psi}$ is commonly measured as

$$L_E = |\boldsymbol{\psi}| = \sqrt{\boldsymbol{\psi}^{\mathbf{T}}\boldsymbol{\psi}}. \tag{4}$$

The length L_E given by equation (4) is dependent on the number of components of vector $\boldsymbol{\psi}$ and it has the same units as the mode shape.

Aenlle et al. [29, 30] defined a new concept of length of a continuous mode shape, which does not coincide with the length of a vector in a Euclidean space that is normally used in linear algebra. This concept was also extended to discrete systems, introducing the concept of a volume matrix. This new definition allows for a better interpretation of the modal mass. In constant mass density systems, the modal mass is equal to the total mass of the structure when the mode shapes are normalized to the unit length, whereas the concept of apparent mass (different for each mode and dependent on the mass distribution) was proposed for nonconstant mass density systems.

In this paper, the concept of cross-length between mode shapes is formulated for continuous systems and later extended to discrete cases by introducing the concept of length matrix. It is demonstrated that in constant mass density systems, the cross-length is zero for all the modes. If the structure is constituted by two parts with different mass density, the ratio of the partial cross-lengths over the two volumes is constant for all the modes and equal to the ratio of the total masses of the respective volumes. The concept of cross-length is used in this paper to determine the accuracy of the modal masses estimated with OMA and EMA. The proposed methodology can also be used to construct a proportional frequency response function (FRF) in constant mass density systems when the modal masses are unknown.

Since finite element programs do not provide the lengths and cross-lengths of the mode shapes, an approximate equation for calculating the length and cross-length of numerical mode shapes is proposed in this paper. Then, this methodology was extended to experimental systems using the structural dynamic modification theory.

Additionally, this methodology can also be applied as a correlation technique. Model correlation techniques are methods used to compare two different models, typically a numerical model and an experimental model. Numerous techniques have been proposed in the literature [33–35], but the most used methods are those based on comparing eigenvalues and eigenvectors. However, no techniques have been proposed to determine whether the discrepancies are in terms of mass, stiffness, or both. In this paper, the cross-length is used to determine how the mass is distributed in the structure and to identify the discrepancies in terms of mass between numerical and experimental models.

The paper is organized as follows: following the introduction, Section 2 presents the basic theory and the equations regarding the length of mode shapes and modal mass in constant and nonconstant mass density systems. In Section 3, the concept of cross-length of mode shapes is defined for both constant and nonconstant mass density systems, which enables the identification of how the mass is distributed in the structure. Approximate equations to calculate the length and the cross-length in numerical and experimental systems are proposed in Section 4. From the concept of cross-length, several important properties are derived in Section 5 for constant mass density systems, which can be used to validate results obtained through experimental and operational modal analyses. The concepts and the equations proposed in this paper were validated in two experimental systems. The results of the numerical models and the experimental tests carried out on an L-shaped steel structure and a T-shaped structure made of steel and wood are presented in Section 6. The paper concludes by summarizing the main findings in Section 7.

2. State of the Art

2.1. Length of Mode Shapes. In [29, 30], the squared length L_i^2 of a continuous mode shape $\boldsymbol{\psi}_\mathbf{i}$ was defined as the average of the length squared $|\boldsymbol{\psi}_\mathbf{i}|^2$ of the mode shape over the considered volume V

$$L_i^2 = \frac{1}{V}\int_{\mathbf{V}} \left|\boldsymbol{\psi}_\mathbf{i}\right|^2 \mathrm{d}V, \tag{5}$$

where V is the total volume of the system. When equation (5) is used, both the length and the mode shapes have the same units.

The continuous formulation was extended to discrete systems in matrix form as [29, 30]

$$L_i^2 = \frac{1}{V}\,\boldsymbol{\psi}_\mathbf{i}^\mathbf{T}\mathbf{V}\boldsymbol{\psi}_\mathbf{i}. \tag{6}$$

If the structure is constituted by two parts with two volumes V_a and V_b with mass densities ρ_a and ρ_b, respectively, equation (6) can also be expressed as [29, 30]

$$L_i^2 V = L_{ia}^2 V_a + L_{ib}^2 V_b, \tag{7}$$

where

$$\begin{aligned} V &= V_a + V_b, \\ L_{ia}^2 &= \frac{1}{V_a}\int_{\mathbf{V_a}} \left|\boldsymbol{\psi}_{\mathbf{V_{ia}}}\right|^2 dV; \quad L_{ib}^2 = \frac{1}{V_b}\int_{\mathbf{V_b}} \left|\boldsymbol{\psi}_{\mathbf{V_{ib}}}\right|^2 \mathrm{d}V, \end{aligned} \tag{8}$$

are the partial lengths, now defined over the partial volumes V_a and V_b, respectively.

In discrete systems, equation (7) still holds, and the expressions of the partial lengths are given by [29, 30]

$$L_{ia}^2 = \frac{1}{V_a}\,\boldsymbol{\psi}_\mathbf{ia}^\mathbf{T}\mathbf{V}\boldsymbol{\psi}_\mathbf{ia}; \quad L_{ib}^2 = \frac{1}{V_b}\,\boldsymbol{\psi}_\mathbf{ib}^\mathbf{T}\mathbf{V}\boldsymbol{\psi}_\mathbf{ib}. \tag{9}$$

Equation (7) easily generalizes to cases with many "q" volumes with constant mass density, i.e., [29, 30]

$$L_i^2 V = \sum_q L_{iq}^2 V_q. \tag{10}$$

2.2. Modal Mass in Constant and Nonconstant Mass Density Systems. The modal mass for a continuous system with constant mass density is defined as [29, 30, 36, 37]

$$m_i = \int_{\mathbf{V}} \rho \left|\boldsymbol{\psi}_\mathbf{i}\right|^2 \mathrm{d}V. \tag{11}$$

It can also be expressed as

$$m_i = \rho V \frac{1}{V}\int_{\mathbf{V}} \left|\boldsymbol{\psi}_\mathbf{i}\right|^2 \mathrm{d}V = M L_i^2, \tag{12}$$

where $M = \rho V$ is the total mass of the system. The same expression is obtained for discrete systems as

$$m_i = \boldsymbol{\psi}_\mathbf{i}^\mathbf{T}\mathbf{M}\boldsymbol{\psi}_\mathbf{i} = \rho V \frac{1}{V}\boldsymbol{\psi}_\mathbf{i}^\mathbf{T}\mathbf{V}\boldsymbol{\psi}_\mathbf{i} = M L_i^2. \tag{13}$$

If the structure consists of two volumes, V_a with the mass density ρ_a and V_b with the mass density ρ_b, the modal mass can be formulated as [29, 30]

$$m_i = \frac{V_a}{V_a}\int_{\mathbf{V_a}} \rho_a \left|\boldsymbol{\psi}_{\mathbf{V_{ia}}}\right|^2 dV + \frac{V_b}{V_b}\int_{\mathbf{V_b}} \rho_b \left|\boldsymbol{\psi}_{\mathbf{V_{ib}}}\right|^2 dV = M_a L_{ia}^2 + M_b L_{ib}^2, \tag{14}$$

where

$$M = M_a + M_b. \tag{15}$$

Equation (14) shows that the modal mass can be obtained as the summation of the partial lengths defined over the partial volumes weighed with the total mass of each volume. Equation (14) can be easily generalized to "q" volumes as [29, 30]

$$m_i = \sum_q M_q L_{iq}^2. \tag{16}$$

3. The Concept of Cross-Length of Mode Shapes

If a mode shape $\boldsymbol{\psi}$ has three components $\boldsymbol{\psi}_\mathbf{x}, \boldsymbol{\psi}_\mathbf{y}, \boldsymbol{\psi}_\mathbf{z}$, the Euclidean length is given by

$$|\boldsymbol{\psi}| = \sqrt{\boldsymbol{\psi}_\mathbf{x}^2 + \boldsymbol{\psi}_\mathbf{y}^2 + \boldsymbol{\psi}_\mathbf{z}^2}. \tag{17}$$

The continuous cross-length L_{ij} between the mode shapes $\boldsymbol{\psi}_\mathbf{i}$ and $\boldsymbol{\psi}_\mathbf{j}$ is defined as

$$L_{ij} = \frac{1}{V}\int_{\mathbf{V}} \sqrt{\boldsymbol{\psi}_\mathbf{xi}^2\boldsymbol{\psi}_\mathbf{xj}^2 + \boldsymbol{\psi}_\mathbf{yi}^2\boldsymbol{\psi}_\mathbf{yj}^2 + \boldsymbol{\psi}_\mathbf{zi}^2\boldsymbol{\psi}_\mathbf{zj}^2}\,\mathrm{d}V, \tag{18}$$

which has the same units as the mode shape.

On the other hand, the discrete formulation of the squared cross-length L_{ij} in matrix form is given by

$$L_{ij}^2 = \frac{1}{V}\,\boldsymbol{\psi}_\mathbf{i}^\mathbf{T}\mathbf{V}\boldsymbol{\psi}_\mathbf{j}, \quad i \neq j. \tag{19}$$

A length matrix $\mathbf{L}^2$ containing the squared lengths in the diagonal terms, and the squared cross-lengths in the off-diagonal terms, can be obtained by means of the expression

$$\mathbf{L}^\mathbf{2} = \frac{1}{V}\,\boldsymbol{\psi}^\mathbf{T}\mathbf{V}\boldsymbol{\psi}. \tag{20}$$

3.1. Cross-Length in Constant Mass Density Systems. The orthogonality of the mode shapes $\boldsymbol{\psi}_\mathbf{i}$ and $\boldsymbol{\psi}_\mathbf{j}$ with respect to the mass matrix is given by

$$m_{ij} = \boldsymbol{\psi}_\mathbf{i}^\mathbf{T}\mathbf{M}\boldsymbol{\psi}_\mathbf{j} = 0, \quad i \neq j. \tag{21}$$

In constant mass density systems, equation (21) can also be expressed as

$$m_{ij} = \rho V \frac{1}{V} \boldsymbol{\psi}_{\mathbf{i}}^{\mathbf{T}} \mathbf{V} \boldsymbol{\psi}_{\mathbf{j}} = M L_{ij}^2 = 0 \quad i \neq j, \tag{22}$$

from which it is inferred that

$$L_{ij}^2 = 0, \quad i \neq j, \tag{23}$$

i.e., in constant mass density systems, the cross-length is zero for all the modes and, consequently, the length matrix $\mathbf{L^2}$ is diagonal.

3.2. Cross-Length in Nonconstant Mass Density Systems. If the structure consists of two volumes V_a and V_b, the cross-length between the mode shapes $\boldsymbol{\psi}_{\mathbf{i}}$ and $\boldsymbol{\psi}_{\mathbf{j}}$ can be expressed as

$$L_{ij}^2 V = L_{ija}^2 V_a + L_{ijb}^2 V_b, \quad i \neq j, \tag{24}$$

where L_{ija}^2 and L_{ijb}^2 are the squared partial cross-lengths calculated over the two volumes, V_a and V_b, respectively.

The orthogonality of the mode shapes $\boldsymbol{\psi}_{\mathbf{i}}$ and $\boldsymbol{\psi}_{\mathbf{j}}$ with respect to the mass matrix results in

$$m_{ij} = M_a L_{\mathrm{ija}}^2 + M_b L_{\mathrm{ijb}}^2 = 0, \quad i \neq j, \tag{25}$$

from which the following relationship between total masses and the squared cross-lengths is derived:

$$\frac{M_a}{M_b} = -\frac{L_{ijb}^2}{L_{ija}^2}, \quad i \neq j. \tag{26}$$

From equation (26), it is inferred that the ratio of the partial cross-lengths over the volumes V_a and V_b, is constant for all the modes and equal to the ratio of the total masses of such volumes.

The generalization of equations (24) and (25) to "q" volumes leads to

$$\begin{aligned} L_{ij}^2 V &= \sum_q L_{\mathrm{ijq}}^2 V_q, \\ \sum_q L_{\mathrm{ijq}}^2 M_q &= 0, \end{aligned} \tag{27}$$

respectively.

4. Length and Cross-Length of Numerical and Experimental Mode Shapes

Finite element programs do not provide the lengths and the cross-lengths of the mode shapes given by equations (6) and (19). Although the mode shapes can be exported from finite element programs, this is not the case with the volume matrices and, consequently, the lengths and the cross-lengths cannot be calculated in an external application either.

If a structural numerical model is discretized with N_V finite elements of small volume ΔV, the squared length of a numerical mode shape $\boldsymbol{\psi}_{\mathbf{FEi}}$ can be accurately approximated by

$$L_{\mathrm{FEi}}^2 \cong \frac{\sum_{k=1}^{N_V} \Delta V_K \boldsymbol{\psi}_{\mathrm{FEki}}^2}{\sum_{k=1}^{N_V} \Delta V_K}, \tag{28}$$

where $\boldsymbol{\psi}_{\mathrm{FEki}}$ is the k-th component of mode shape $\boldsymbol{\psi}_{\mathbf{FEi}}$ at the centroid of the volume ΔV_k. If all the elements have the same volume ΔV, equation (28) results in

$$L_{\mathrm{FEi}}^2 \cong \frac{\sum_{k=1}^{N_V} \boldsymbol{\psi}_{\mathrm{FEki}}^2}{N_V}. \tag{29}$$

As the components of the mode shapes are commonly known at the nodes of the elements, the squared length of the i-th mode shape $\boldsymbol{\psi}_{\mathrm{FEi}}$ can be approximated by means of the expression

$$L_{\mathrm{FEi}}^2 \cong \frac{\boldsymbol{\psi}_{\mathbf{FEi}}^{\mathbf{T}} \boldsymbol{\psi}_{\mathbf{FEi}}}{N}, \tag{30}$$

where N is the number of nodes in the model.

Similarly, the squared cross-length L_{ij}^2 between the mode shapes $\boldsymbol{\psi}_{\mathbf{i}}$ and $\boldsymbol{\psi}_{\mathbf{j}}$ can be approximated by

$$L_{\mathrm{FEij}}^2 = \frac{\boldsymbol{\psi}_{\mathbf{FEi}}^{\mathbf{T}} \boldsymbol{\psi}_{\mathbf{FEj}}}{N}. \tag{31}$$

A length matrix $\mathbf{L_{FE}^2}$ containing the square lengths in the diagonal terms and the square cross-lengths in the off-diagonal terms can be obtained by means of the expression

$$\mathbf{L_{FE}^2} \cong \frac{\boldsymbol{\psi}_{\mathbf{FE}}^{\mathbf{T}} \boldsymbol{\psi}_{\mathbf{FE}}}{N}. \tag{32}$$

According to the structural dynamic modification theory, the experimental mode shapes can be expressed as a linear combination of the numerical ones $\boldsymbol{\psi}_{\mathbf{FE}}$ [38–40] using the expression

$$\boldsymbol{\psi}_{\mathbf{X}} = \boldsymbol{\psi}_{\mathbf{FE}} \mathbf{T}, \tag{33}$$

where $\mathbf{T}$ is a transformation matrix. Since the experimental mode shapes are only known at the measured or active DOFs, an approximation of matrix $\mathbf{T}$ can be obtained by

$$\mathbf{T} = \boldsymbol{\psi}_{\mathbf{FEa}}^{+} \boldsymbol{\psi}_{\mathbf{Xa}}, \tag{34}$$

where subindex "a" indicates active or measured DOFs and superindex "+" indicates pseudoinverse.

Assuming that the experimental system is discretized with the same number of volumes as the numerical model, the matrix with the experimental squared lengths and cross-lengths $\mathbf{L_X^2}$ can be obtained by means of the expression

$$\mathbf{L_X^2} \cong \frac{\boldsymbol{\psi}_{\mathbf{X}}^{\mathbf{T}} \boldsymbol{\psi}_{\mathbf{X}}}{N}. \tag{35}$$

Substituting equation (33) in (35) leads to

$$\mathbf{L_X^2} \cong \frac{\mathbf{T}^{\mathbf{T}} \boldsymbol{\psi}_{\mathbf{FE}}^{\mathbf{T}} \boldsymbol{\psi}_{\mathbf{FE}} \mathbf{T}}{N} = \mathbf{T}^{\mathbf{T}} \mathbf{L_{FE}^2} \mathbf{T}. \tag{36}$$

5. Implications of Constant Mass Density

Several important properties for constant mass density systems are derived from the equations presented in Sections 2 and 3. These properties can be used to validate results obtained with experimental and operational modal analysis and to construct proportional frequency response functions and proportional change flexibility matrices.

5.1. Relation between Modal Masses. From (12), it is inferred that the modal masses of a dynamic system with constant mass density are related through the equation by

$$\frac{m_1}{L_1^2} = \frac{m_2}{L_2^2} \ldots = \frac{m_r}{L_r^2} = \ldots = M. \tag{37}$$

This means that if the modal mass of one mode is known, the modal masses of the remaining modes can be estimated with equation (37).

5.2. Relation between Modal Masses. The frequency response function (FRF) in terms of modal parameters, in case of proportional damping, is given by

$$\mathbf{H}(\boldsymbol{\omega}) = \sum_{\mathbf{r=1}}^{\mathbf{N}} \frac{\boldsymbol{\psi}_\mathbf{r}\boldsymbol{\psi}_\mathbf{r}^\mathbf{T}}{m_r\left(\omega_r^2 - \omega^2 + i2\zeta_r\omega\omega_r\right)}, \tag{38}$$

where ω is the frequency, and $\omega_r, \zeta_r,$ andm_r are the natural frequency, damping ratio, and modal mass of the r-th mode, respectively. If equation (37) is substituted in equation (38), the resulting equation is

$$\mathbf{H}(\boldsymbol{\omega}) = \frac{1}{M}\sum_{\mathbf{r=1}}^{\mathbf{N}} \frac{\boldsymbol{\psi}_\mathbf{r}\boldsymbol{\psi}_\mathbf{r}^\mathbf{T}}{L_r^2\left(\omega_r^2 - \omega^2 + i2\zeta_r\omega\omega_r\right)}. \tag{39}$$

This means that a proportional FRF can be constructed without knowing the modal masses, i.e., only the squared lengths of the mode shapes are needed.

5.3. Change in Flexibility Matrix. The flexibility matrix $\mathbf{f}$, in terms of modal parameters, is expressed as

$$\mathbf{f} = \frac{1}{M}\sum_{\mathbf{r=1}}^{\mathbf{N}} \frac{\boldsymbol{\psi}_\mathbf{r}\boldsymbol{\psi}_\mathbf{r}^\mathbf{T}}{L^2\omega_r^2}. \tag{40}$$

If we consider two different states of an experimental structure, damaged denoted here with the subindex "D" and undamaged, denoted here with subindex "U", the change in flexibility matrix is given by

$$\Delta\mathbf{f} = \sum_{\mathbf{r=1}}^{\mathbf{N}} \frac{\boldsymbol{\psi}_{\mathbf{XDr}}\boldsymbol{\psi}_{\mathbf{XDr}}^\mathbf{T}}{m_{XDr}\omega_{XDr}^2} - \sum_{\mathbf{r=1}}^{\mathbf{N}} \frac{\boldsymbol{\psi}_{\mathbf{XUr}}\boldsymbol{\psi}_{\mathbf{XUr}}^\mathbf{T}}{m_{XUr}\omega_{XUr}^2}, \tag{41}$$

where subindex "X" indicates experimental.

If we assume that there are no changes in terms of mass between both states, i.e., the total mass M is the same for both states, the following equation can be expressed as

$$\begin{aligned}\Delta\mathbf{f} &= \frac{1}{M}\sum_{\mathbf{r=1}}^{\mathbf{N}} \frac{\boldsymbol{\psi}_{\mathbf{XDr}}\boldsymbol{\psi}_{\mathbf{XDr}}^\mathbf{T}}{L_{XDr}^2\omega_{XDr}^2} - \frac{\mathbf{1}}{M}\sum_{\mathbf{r=1}}^{\mathbf{N}} \frac{\boldsymbol{\psi}_{\mathbf{XUr}}\boldsymbol{\psi}_{\mathbf{XUr}}^\mathbf{T}}{L_{XUr}^2\omega_{XUr}^2},\\ \Delta\mathbf{f} &= \frac{1}{M}\left[\sum_{\mathbf{r=1}}^{\mathbf{N}} \frac{\boldsymbol{\psi}_{\mathbf{XDr}}\boldsymbol{\psi}_{\mathbf{XDr}}^\mathbf{T}}{L_{XDr}^2\omega_{XDr}^2} - \sum_{\mathbf{r=1}}^{\mathbf{N}} \frac{\boldsymbol{\psi}_{\mathbf{XUr}}\boldsymbol{\psi}_{\mathbf{XUr}}^\mathbf{T}}{L_{XUr}^2\omega_{XUr}^2}\right],\end{aligned} \tag{42}$$

i.e., a proportional change flexibility matrix can also be constructed without knowing the modal masses.

Moreover, as there are no changes in mass, the modal mass matrix of the damage system can be obtained by

$$\mathbf{m_{XD}} = \mathbf{T}^\mathbf{T}\mathbf{m_{XU}}\mathbf{T}, \tag{43}$$

where $\mathbf{T}$ is a transformation matrix, which relates the mode shapes $\boldsymbol{\psi}_\mathbf{XD}$ and $\boldsymbol{\psi}_\mathbf{XU}$ by

$$\boldsymbol{\psi}_\mathbf{XD} = \boldsymbol{\psi}_\mathbf{XU}\,\mathbf{T}. \tag{44}$$

Substitution of equation (12) in (43) results in

$$M\mathbf{L}_\mathbf{XD}^\mathbf{2} = M\mathbf{T}^\mathbf{T}\mathbf{L}_\mathbf{XU}^\mathbf{2}\mathbf{T}, \tag{45}$$

i.e., the squared length matrix of the damage and undamaged mode shapes are related by

$$\mathbf{L}_\mathbf{XD}^\mathbf{2} = \mathbf{T}^\mathbf{T}\mathbf{L}_\mathbf{XU}^\mathbf{2}\mathbf{T}. \tag{46}$$

5.4. Mass Change Method. When the mass change method is used to estimate the modal masses in operational modal analysis, the following equation can be used [5, 31]:

$$m_i = \frac{\boldsymbol{\psi}_\mathbf{Oi}^\mathbf{T}\Delta\mathbf{M}\boldsymbol{\psi}_\mathbf{Ii}}{\left(\omega_{Oi}^2/\omega_{Ii}^2 - 1\right)B_{ii}}, \tag{47}$$

where subindexes "0" and "I" refer to unperturbed and perturbed systems, respectively. $\Delta\mathbf{M}$ is the mass change matrix, and B_{ii} is the i-th diagonal entry of the matrix $\mathbf{B}$ defined as

$$\mathbf{B} = \boldsymbol{\psi}_\mathbf{0}^+\boldsymbol{\psi}_\mathbf{I}. \tag{48}$$

Substituting (12) in (47) yields

$$\frac{\boldsymbol{\psi}_\mathbf{Oi}^\mathbf{T}\Delta\mathbf{M}\boldsymbol{\psi}_\mathbf{Ii}}{\left(\omega_{Oi}^2/\omega_{Ii}^2 - 1\right)B_{ii}L_i^2} = \ldots = \frac{\boldsymbol{\psi}_\mathbf{Or}^\mathbf{T}\Delta\mathbf{M}\boldsymbol{\psi}_\mathbf{Ir}}{\left(\omega_{Or}^2/\omega_{Ir}^2 - 1\right)B_{rr}L_r^2} = \ldots = M. \tag{49}$$

6. Experimental Examples

6.1. An L-Shaped Steel Structure. A steel structure with L-shape, consisting of a vertical column with a height of 1. 46 m and a horizontal beam that is 0.615 m long, was considered in this study. Both the vertical column and the horizontal beam have a rectangular hollow steel section of 8 cm × 4 cm and a thickness of 4mm. The structure was fixed at the bottom of the column (see Figure 1), and its total mass was $M_X = 13.42\,kg$.

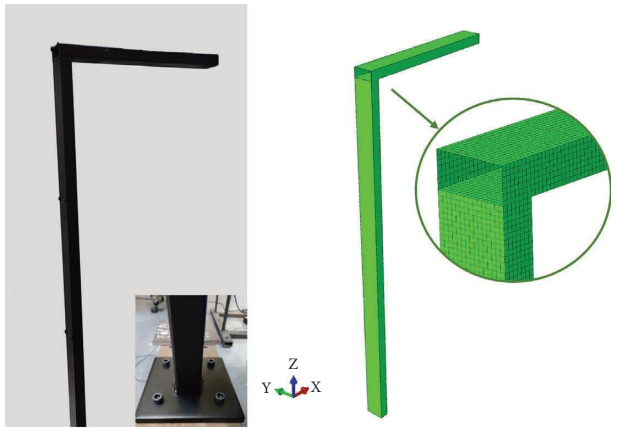

Figure 1: The steel structure used in the experiments.

A numerical model of the structure was assembled in ABAQUS [41] and meshed with shell elements S8R (8 nodes with reduced integration) using a global size of 0.005 m (see Figure 1). A fixed support was considered at the bottom of the column. The following mechanical properties were considered for the steel: mass density $\varrho = 7850\,kg/m3$, Young's modulus $E = 210{\bullet}10^9\ N/m2$, and Poisson's ratio $\nu = 0.3$. The total mass of the numerical model was $M_{FE} = 14.59$ kg.

The numerical natural frequencies f_{FE} and the modal masses m_{FE} corresponding to the first eight modes, extracted with a frequency analysis, are shown in Tables 1 and 2, respectively. The mode shapes were normalized to the largest component equal to unity and are presented in Figure 2.

The experimental modal parameters were first estimated with operational modal analysis (OMA). The structure was excited by applying many small random hits using the hands [25], and the responses were measured at fifteen points using twelve accelerometers (two data sets) with a sensitivity of 100 mV/g. The test setup is shown in Figure 3, where the arrows indicate the measured directions.

The responses were recorded for approximately 4 minutes using a sampling frequency of 2132 Hz [42]. The singular value decomposition of the experimental responses is presented in Figure 4. The modal parameters of the first 8 modes were estimated with the stochastic subspace iteration (SSI) [25] technique, and the natural frequencies are presented in Table 1.

The modal parameters were also estimated with experimental modal analysis, using the same sensors, instrumentation, and test setup as those used in OMA. The structure was excited with an impact hammer applying the forces in DOFs 10, 11, and 12, respectively (see Figure 3). The modal parameters were estimated with the complex mode indication function (CMIF) technique [22–24]. The natural frequencies are presented in Table 1 and the modal masses estimated by EMA (m_{X3}) are shown in Table 2.

The numerical $\mathbf{L}^2_{\mathbf{FE}}$ and experimental $\mathbf{L}^2_{\mathbf{X}}$ squared length matrices estimated with equations (32) and (35), respectively, are shown in Tables3 and 4.

Although there are significant discrepancies between the experimental and the numerical models, the latter was not updated in order to show the robustness of the equations proposed in this paper.

Table 1: Natural frequencies (Hz).

Mode	Natural frequencies (Hz)			Error (%)	
	FE model	OMA (SSI)	EMA	FE-OMA	FE-EMA
1	12.53	10.945	10.938	14.48	14.55
2	20.85	18.953	18.75	10.01	11.20
3	55.74	50.995	50.781	9.30	9.77
4	55.31	54.39	54.688	1.69	1.14
5	131.98	115.485	115.625	14.28	14.14
6	198.10	179.742	180.469	10.21	9.77
7	324.78	283.539	284.572	14.55	14.13
8	502.56	464.154	465.35	8.27	8.00

Table 2: Modal masses (kg) of the L-shape structure. Mode shapes normalized to the largest component equal to unity.

Mode	Modal masses (kg)			
	$\mathbf{m_{FE}}$	$\mathbf{m_{X1}} = \mathbf{M_{Tx}L_x^2}$	$\mathbf{m_{X2}} = \mathbf{T^TT}$	$\mathbf{m_{X3}}$ EMA
1	6.9033	6.3732	6.9460	6.25
2	3.6589	3.7333	4.0540	3.74
3	1.7099	1.5769	1.7082	1.47
4	2.0423	1.8854	2.0390	1.87
5	7.1208	6.5764	7.1831	6.57
6	5.6175	5.1591	5.6162	5.51
7	5.4204	4.8506	5.3671	4.93
8	5.6316	4.2968	4.6581	4.18

The modal masses were also estimated with the equation proposed in [21]:

$$\mathbf{m_{X2}} = \mathbf{T^TT}, \tag{50}$$

where matrix $\mathbf{T}$ must be estimated using mass-normalized numerical mode shapes and unscaled experimental mode shapes.

Since the total mass of the experimental structure is known, the modal masses were also estimated with equation (13) (m_{X1} in Table 2), using the experimental square length matrix $\mathbf{L}^2_{\mathbf{X}}$.

6.1.1. Discussion. The discrepancies in terms of natural frequencies between the numerical and experimental models are in the range 0–15%. The modal assurance criteria (MAC) [34, 35] (see Table 5) give diagonal values over 0.9795, which indicates a good correlation in terms of mode shapes; however, high off-diagonal values have been obtained.

The errors in modal masses obtained using different techniques described in the previous section, are shown in Table 6. The maximum error between m_{X1} and m_{X3} is 7%, which indicates that the squared length L^2_X has been estimated with good accuracy using equation (35), although there are significant discrepancies between the numerical and the experimental models.

Since the mass density of this structure is constant, the modal masses corresponding to each mode shape are related through equation (37). The ratio modal mass/squared length is presented in Table 7 and the errors are shown in Table 8. The ratios m_{FE}/L^2_{FE} are, as expected, very close to the total mass $M_{FE} = 14.59$ kg of the numerical model for all the

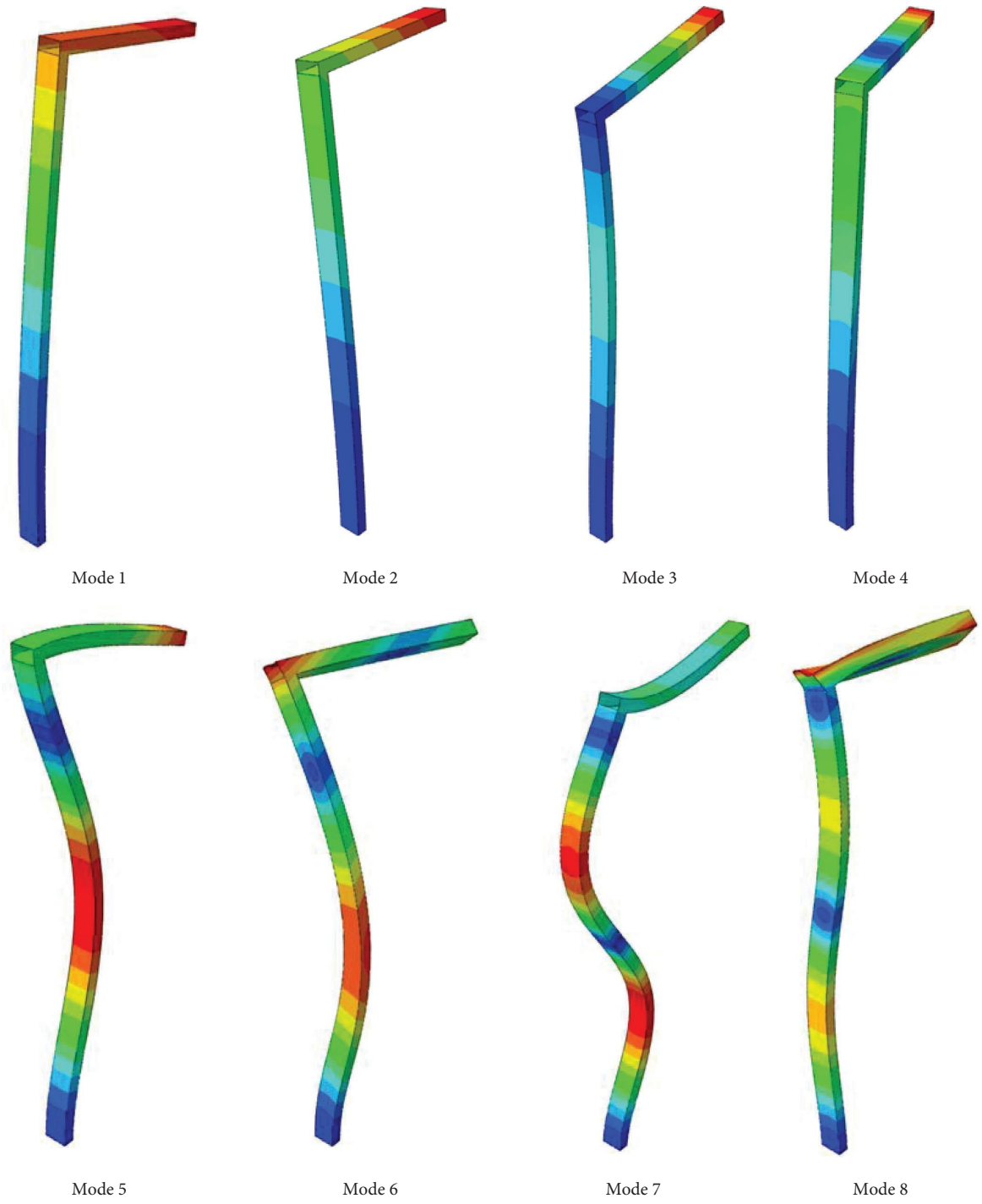

Figure 2: Numerical mode shapes of the L steel structure.

modes, with discrepancies being less than 1% (see Table 8). In this case, the ratios are not exactly equal to $M_{FE} = 14.59\,\text{kg}$ because the length of the numerical mode shapes is estimated using (32), which is an approximation.

The ratio m_{X1}/L_X^2 coincides with $M_X = 13.42\,\text{kg}$ because M_X is used in equation (13).

The maximum discrepancies between m_{X2}/L_X^2 and $M_X = 13.42\,kg$ are in the range 8.15–10.65%. The accuracy of equation (50) (m_{X2}) depends on the correlation, in terms of mass, between the numerical and experimental models. Since there is a discrepancy of approximately 10% between the total masses of both the (experimental and numerical) models, it is expected to have errors of the same order in the modal masses estimated with equation (50). On the other hand, the ratio m_{X2}/L_X^2 is very close to $M_{FE} = 14.59\,kg$ for all the modes, with the maximum discrepancy being less than 1.77%.

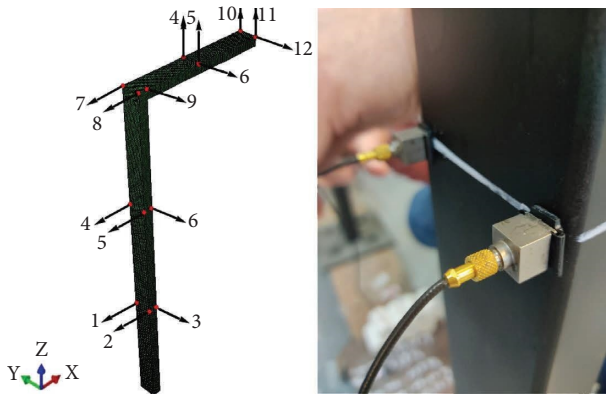

Figure 3: Test setup for both operational and experimental modal analyses.

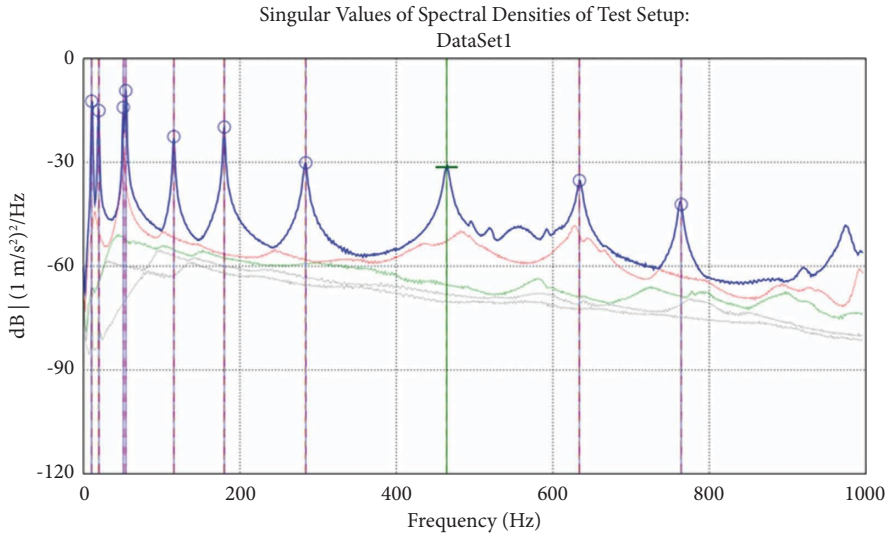

Figure 4: Singular value decomposition of the responses.

A better correlation exists between M_X and m_{X3}/L_X^2 (modal masses estimated with experimental modal analysis), with the discrepancies being less than 7% for all the modes with $M_X = 13.42\,kg$.

In constant mass density systems, there exists a relationship given by (37) between the modal masses of different modes. This information can be used to validate the modal masses estimated through modal analysis (or by combining numerical models with modal analysis). The accuracy of the presented results can be improved by achieving a better correlation between the numerical and the experimental models.

6.2. A T Steel-Wood Structure. This structure consists of a vertical steel column (height 1.70 m) with a rectangular hollow steel section of 8 cm × 4 cm and thickness of 4mm, and a horizontal wooden beam (length 2 m) with rectangular section of 12.7 cm × 7 cm (see Figure 5). The structure is fixed at the bottom of the column, and a steel plate was welded at the top of the column to connect it to the wooden beam using four bolts. The total mass of the steel part is M_{XS} = 11.96Kg and that of the wooden part is M_{XW} = 11.46Kg.

A finite element model was assembled in ABAQUS [41] using the geometrical parameters described in the previous paragraph and meshed with 3D elements (20 nodes with reduced integration). The following mechanical properties were considered for the steel: mass density $\varrho = 7850\,\text{kg}/m3$, total mass $M_{\text{FES}} = 13.02\,\text{kg}$, Young's modulus $E = 210{\bullet}10^9\,N/m2$, and Poisson's ratio $\nu = 0.3$. For the wood, the following properties were considered: mass density $\varrho = 644\,\text{kg}/m3$, total mass $M_{\text{FEW}} = 11.46\,\text{kg}$, Young's modulus $E = 13.5{\bullet}10^9\,N/m2$, and Poisson's ratio $\nu = 0.38$. The numerical natural frequency f_{FE} and modal masses m_{FE} are presented in Tables 9 and 10, respectively.

The experimental modal parameters were estimated with experimental and operational modal analysis. In OMA, the responses were recorded for approximately 4 minutes with a sampling frequency of 1632 Hz using two data sets (see Figure 6). The responses were measured at twenty-one points using fifteen accelerometers (100 mV/g) using the same data acquisition system as that used in the L structure. The singular value decomposition of the experimental responses is presented in Figure 7, and the modal parameters

Table 3: Squared length of the first 8 numerical mode shapes of the L steel structure.

		Mode							
		1	2	3	4	5	6	7	8
Mode	1	0.4734	0.0000	0.0000	−0.0006	0.0001	0.0000	0.0000	0.0000
	2	0.0000	0.2512	0.0010	0.0000	0.0000	−0.0005	0.0000	−0.0002
	3	0.0000	0.0010	0.1407	0.0000	0.0000	−0.0005	0.0000	−0.0006
	4	−0.0006	0.0000	0.0000	0.1179	−0.0008	0.0000	0.0004	0.0000
	5	0.0001	0.0000	0.0000	−0.0008	0.4882	0.0000	−0.0005	0.0000
	6	0.0000	−0.0005	−0.0005	0.0000	0.0000	0.3848	0.0000	0.0009
	7	0.0000	0.0000	0.0000	0.0004	−0.0005	0.0000	0.3711	0.0000
	8	0.0000	−0.0002	−0.0006	0.0000	0.0000	0.0009	0.0000	0.3876

Table 4: Squared length of the first 8 experimental mode shapes of the L steel structure.

		Mode							
		1	2	3	4	5	6	7	8
Mode	1	0.4749	0.0116	0.0000	−0.0124	0.00000	0.0123	0.0125	0.0134
	2	0.0116	0.2782	0.0020	−0.0044	0.0046	0.0054	0.0014	0.0032
	3	0.0000	0.0020	0.1175	−0.0014	0.0000	0.0000	0.0070	0.0065
	4	−0.0124	−0.0044	−0.0014	0.1405	−0.0037	−0.0021	0.0000	−0.0016
	5	0.0000	0.0046	0.0000	−0.0037	0.4900	0.0159	−0.0014	0.0157
	6	0.0123	0.0054	0.0000	−0.0021	0.0159	0.3844	−0.0028	0.0000
	7	0.0125	0.0014	0.0070	0.0000	−0.0014	−0.0028	0.3614	−0.0171
	8	0.0134	0.0032	0.0065	−0.0016	0.0157	0.0000	−0.0171	0.3202

Table 5: Modal assurance criteria (MAC) of the L steel structure.

MAC							
0.9959	0.0003	0.1083	0.0005	0.1178	0.0000	0.0105	0.0000
0.0012	0.9960	0.0003	0.1167	0.0000	0.0051	0.0000	0.0825
0.1490	0.0002	0.9987	0.0001	0.1510	0.0000	0.0500	0.0000
0.0001	0.1590	0.0007	0.9972	0.0006	0.0893	0.0001	0.0447
0.1013	0.0000	0.1764	0.0000	0.9935	0.0002	0.0084	0.0000
0.0009	0.0039	0.0000	0.1204	0.0000	0.9927	0.0001	0.1524
0.0172	0.0000	0.0234	0.0000	0.0425	0.0000	0.9876	0.0001
0.0002	0.0700	0.0041	0.0557	0.0043	0.2200	0.0027	0.9795

Table 6: Errors (%) between modal masses of the L-shape structure.

Mode	Error (%)				
	$\mathbf{m_{FE}}$-$\mathbf{m_{X1}}$	$\mathbf{m_{X2}} - \mathbf{m_{X1}}$	$\mathbf{m_{X1}} - \mathbf{m_{X3}}$	$\mathbf{m_{FE}}$-$\mathbf{m_{X3}}$	$\mathbf{m_{X2}}$-$\mathbf{m_{X3}}$
1	8.32	8.99	1.97	10.45	11.14
2	1.99	8.59	0.18	2.17	8.40
3	8.43	8.33	7.27	16.32	16.20
4	8.32	8.15	0.82	9.21	9.04
5	8.28	9.23	0.10	8.38	9.33
6	8.89	8.86	6.37	1.95	1.93
7	11.75	10.65	1.61	9.95	8.87
8	31.06	8.41	2.79	34.73	11.44

were estimated with the stochastic subspace iteration (SSI) [25].

The modal parameters were also estimated by experimental modal analysis (EMA) using the complex mode indicator function (CMIF) technique. The same sensors, instrumentation, and test setup as those used in OMA were used in the EMA, with the structure excited with an impact hammer applying the forces in DOFs 9, 14, and 15, respectively (see Figure 6).

Table 7: Ratio modal mass/square length.

Mode	Ratio modal mass/square length			
	$\mathbf{m_{FE}}/\mathbf{L_{FE}^2}$	$\mathbf{m_{X1}}/\mathbf{L_X^2}$	$\mathbf{m_{X2}}/\mathbf{L_X^2}$	$\mathbf{m_{X3}}/\mathbf{L_X^2}$
1	14.5815	13.4200	14.6262	13.1607
2	14.5658	13.4200	14.5730	13.4442
3	14.5152	13.4200	14.5367	12.5100
4	14.4991	13.4200	14.5138	13.3107
5	14.5855	13.4200	14.6580	13.4068
6	14.6002	13.4200	14.6091	14.3328
7	14.6066	13.4200	14.8488	13.6395
8	14.5295	13.4200	14.5486	13.0553

Table 8: Errors (%) between the estimated ratio modal mass/squared length and the total mass of the structure.

Mode	Error (%)			
	$\mathbf{m_{FE}}/\mathbf{L_{FE}^2}$ - $\mathbf{M_{FE}}$	$\mathbf{m_{X2}}/\mathbf{L_X^2}$ - $\mathbf{M_{FE}}$	$\mathbf{m_{X2}}/\mathbf{L_X^2}$ - $\mathbf{M_X}$	$\mathbf{m_{X3}}/\mathbf{L_X^2}$ - $\mathbf{M_X}$
1	0.06	0.25	8.99	1.93
2	0.17	0.12	8.59	0.18
3	0.51	0.37	8.32	6.78
4	0.62	0.52	8.15	0.81
5	0.03	0.47	9.23	0.10
6	0.07	0.13	8.86	6.80
7	0.11	1.77	10.65	1.64
8	0.41	0.28	8.41	2.72

The experimental natural frequencies corresponding to the first eight modes are shown in Table 9. The mode shapes are presented in Figure 8.

Figure 5: The T steel-wood structure used in the experiments.

Table 9: Natural frequencies of the T structure.

Mode	Natural frequencies (Hz)			Error (%)	
	FE model	OMA (SSI)	EMA	FE-OMA	FE-EMA
1	6.21	5.284	5.308	17.52	16.99
2	11.89	10.337	10.388	15.02	14.46
3	13.07	12.07	11.79	8.29	10.86
4	24.69	18.883	18.366	30.75	34.43
5	56.07	50.276	50.753	11.52	10.48
6	95.45	76.817	75.258	24.26	26.83
7	110.48	99.966	100.315	10.52	10.13
8	151.47	138.73	140.385	9.18	7.90

Since the total mass of the two parts of the experimental structure is known, the modal masses were estimated with equation (14). This equation can be particularized to the experimental model, resulting in

$$m_{X1} = M_{Xs}L_{Xs}^2 + M_{Xw}L_{Xw}^2. \quad (51)$$

The modal masses estimated by experimental modal analysis (m_{X3}), and those calculated using (50) (m_{X2}), are shown in Table 10.

6.2.1. Discussion. The discrepancies in terms of natural frequencies between the numerical and experimental models are less than 35%. Regarding the MAC [34, 35], the diagonal terms indicate a good correlation, but high values can also be seen in the off-diagonal terms (see Table 11). In this case, the numerical model was also not updated.

Table 10: Modal masses (kg) of the T-shape structure. Mode shapes normalized to the largest component equal to unity.

Mode	Modal masses (kg)			
	$\mathbf{m_{FE}}$	$\mathbf{m_{X1} = M_{XS}L_{XS}^2 + M_{XW}L_{XW}^2}$	$\mathbf{m_{X2} = T^T T}$	$\mathbf{m_{X3}}$ EMA
1	19.5847	18.7063	19.2290	18.90
2	15.4660	14.8818	15.3818	12.87
3	3.8194	3.7901	3.7763	3.698
4	4.6212	4.3718	4.4051	4.329
5	2.7747	2.5442	2.5290	2.79
6	9.5415	7.8577	8.3085	8.75
7	8.5031	8.2197	8.5997	8.16
8	3.9790	3.7832	3.9034	3.77

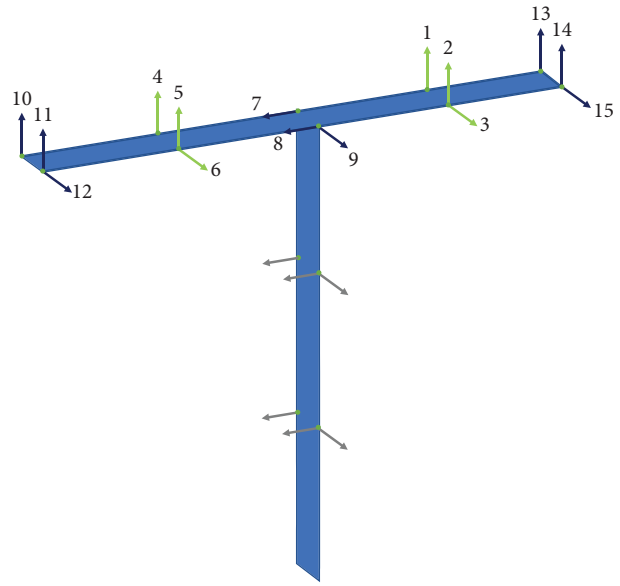

Figure 6: Test setup for the OMA and EMA tests.

The errors in the modal masses obtained with different techniques are shown in Table 12. It can be observed that there is a good agreement between the modal masses m_{X1} and m_{X2}, with discrepancies of less than 6% for all the modes considered in this study. When comparing the values m_{X1} and m_{X3}, larger discrepancies can be found in modes 2 (15.6%), 5 (8.81%), and 6 (10.2%). On the other hand, the largest discrepancies between m_{X2} and m_{X3} correspond to modes 2 (19.52%) and 5 (9.35%).

In this case, the structure consists of two parts made of different materials (wood and steel), and the mass distribution can be obtained using equation (26).

The matrix with the squared lengths and the cross-lengths of the mode shapes, corresponding to the numerical model (mode shapes mass normalized), estimated with equation (32), are shown in Tables 13–15. The matrix with the experimental squared lengths and cross-lengths, estimated with equation (35), are shown in Tables 16–18.

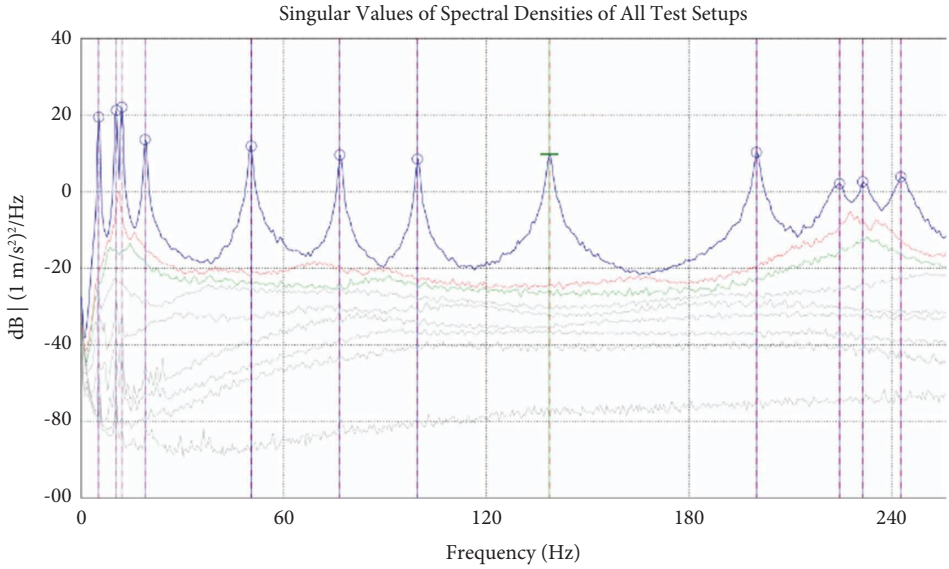

Figure 7: Singular value decomposition of the acceleration responses.

The following overdetermined system of equations is formulated:

$$\begin{bmatrix} L_{Xs}(4,1) & L_{Xw}(4,1) \\ L_{Xs}(6,1) & L_{Xw}(6,1) \\ L_{Xs}(6,4) & L_{Xw}(6,4) \\ L_{Xs}(7,2) & L_{Xw}(7,2) \\ L_{Xs}(8,7) & L_{Xw}(8,7) \end{bmatrix} \begin{bmatrix} M_{Xs} \\ M_{Xw} \end{bmatrix} = \begin{bmatrix} 0 \\ 0 \\ 0 \\ 0 \\ 0 \end{bmatrix}, \tag{52}$$

where the indexes (p,q) indicate the terms of the partial experimental lengths $L_{Xs}(p,q)$ and $L_{Xw}(p,q)$ used to estimate the ratio M_{Xs}/M_{Xw}. In order to reduce the uncertainty, only the terms $L_{Xs}(p,q) > 0.01$ and $L_{Xw}(p,q) > 0.01$have been used.

The least square solution of the system leads to $M_{Xs}/M_{Xw} = 0.9199$. The same system of equations using the numerical model gives $M_{\mathrm{FEs}}/M_{\mathrm{FEw}} = 1.128$.

It is inferred from Table 19 that the squared lengths and cross-lengths have been accurately estimated with equation (26), with an error in the ratio $M_{\mathrm{FEs}}/M_{\mathrm{FEw}}$ of 2.2%. Regarding the experimental ratio M_{Xs}/M_{Xw}, the error is 11.85%.

If the modal masses are known (estimated with experimental modal analysis), equation (14) can be used to estimate the total masses of the two different volumes of the structure. Using the modal masses presented in Table 10 and formulating the system of equations,

$$ZM_X = m_X, \tag{53}$$

where $\mathbf{Z}$ is a matrix containing the diagonal terms of the squared length matrices of the steel ($\mathbf{L^2_{Xs}}$) and the wood ($\mathbf{L^2_{Xw}}$) parts, respectively, i.e.,

$$\mathbf{Z} = \begin{bmatrix} L_{Xs1} & L_{Xw1} \\ L_{Xs2} & L_{Xw2} \\ \vdots & \vdots \end{bmatrix}. \tag{54}$$

$\mathbf{M_X}$ is a vector containing the total masses of the two parts of the structure

$$\mathbf{M_X} = \begin{bmatrix} M_{Xs} \\ M_{Xw} \end{bmatrix}, \tag{55}$$

and $\mathbf{m_X}$ is a vector containing the modal masses, i.e.,

$$\mathbf{m_X} = \begin{bmatrix} m_{X1} \\ m_{X2} \\ \vdots \end{bmatrix}. \tag{56}$$

The values obtained for M_{Xs} and M_{Xw} using (53) are shown in Table 20, together with the residual error obtained with the least squares solution. It can be observed that the masses M_{Xs} and M_{Xw} were estimated with errors less than 6% and 2%, respectively, when using m_{X2}, and with errors less than 6.9% and 6.7%, respectively, when using the modal masses m_{X3}. With respect to the ratio $\mathbf{M_{Xs}/M_{Xw}}$, the error is less than 4% with m_{X2} and less than 14.5% with m_{X3}.

The largest residual error was obtained with modal masses m_{X3} (see Table 20). The estimated errors between the modal masses that have been obtained with the least square solutions and the modal masses m_{X2} and m_{X3} are shown in Figure 9, where it can be observed that less errors have been obtained with m_{X2}. With respect to the discrepancies between the least squares solution and m_{X3}, the larger errors correspond to modes 2 and 5, which can be an indicator that these modal masses were not estimated accurately. This agrees with the results presented in Table 12.

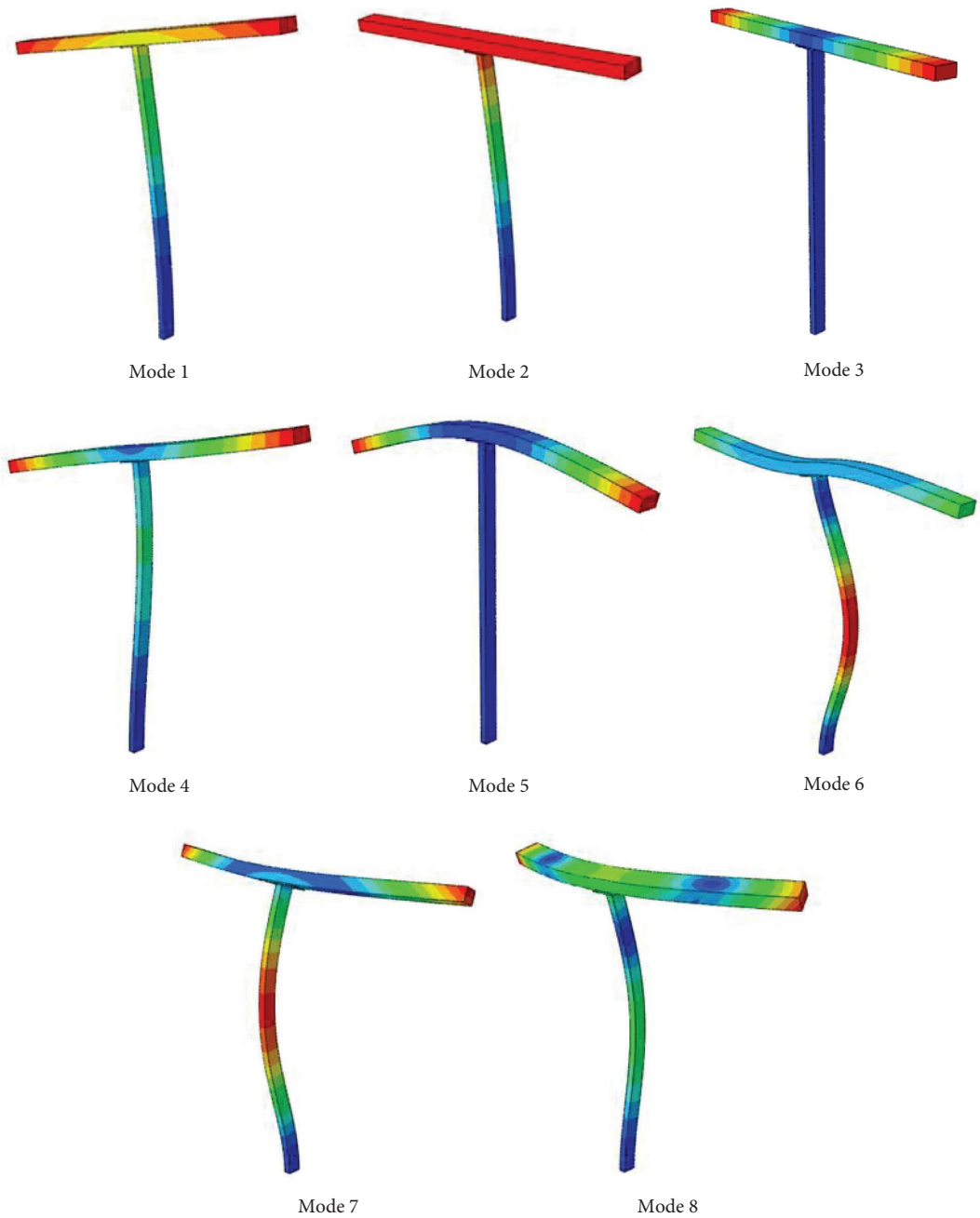

Figure 8: Mode shapes of the T steel-wood structure.

Table 11: Modal assurance criteria (MAC) of the T steel-wood structure.

MAC							
0.9956	0.0001	0.0016	0.3691	0.0002	0.2585	0.0000	0.0001
0.0000	0.9986	0.0001	0.0000	0.0004	0.0000	0.1098	0.2089
0.0004	0.0000	0.9984	0.0005	0.0001	0.0001	0.0001	0.0000
0.4152	0.0002	0.0007	0.9974	0.0002	0.0856	0.0002	0.0002
0.0001	0.0010	0.0006	0.0003	0.9957	0.0000	0.0010	0.0016
0.1673	0.0002	0.0001	0.0182	0.0002	0.9690	0.0000	0.0003
0.0000	0.0735	0.0002	0.0000	0.0010	0.0000	0.9804	0.1105
0.0000	0.2152	0.0001	0.0000	0.0009	0.0000	0.1908	0.9948

Table 12: Errors (%) between modal masses of the T-shape structure.

Mode	Error (%)				
	$\mathbf{m_{FE}}$-$\mathbf{m_{X1}}$	$\mathbf{m_{X2}}$-$\mathbf{m_{X1}}$	$\mathbf{m_{X1}}$-$\mathbf{m_{X3}}$	$\mathbf{m_{FE}}$-$\mathbf{m_{X3}}$	$\mathbf{m_{X2}}$-$\mathbf{m_{X3}}$
1	4.70	2.79	1.02	3.62	1.74
2	3.93	3.36	15.63	20.17	19.52
3	0.77	0.36	2.49	3.28	2.12
4	5.70	0.76	0.99	6.75	1.76
5	9.06	0.60	8.81	0.55	9.35
6	21.43	5.74	10.20	9.05	5.05
7	3.45	4.62	0.73	4.20	5.39
8	5.18	3.18	0.35	5.54	3.54

Table 13: Partial squared length of the first 8 numerical mode shapes estimated with equation (32). Steel Part.

Numerical steel							
0.0141	0.0000	0.0000	0.0117	0.0000	−0.0130	0.0000	0.0000
0.0000	0.0172	0.0000	0.0000	0.0000	0.0000	0.0229	−0.0009
0.0000	0.0000	0.0001	0.0000	0.0000	0.0000	0.0000	0.0000
0.0117	0.0000	0.0000	0.0123	0.0000	−0.0219	0.0000	0.0000
0.0000	0.0000	0.0000	0.0000	0.0000	0.0000	0.0000	0.0000
−0.0130	0.0000	0.0000	−0.0219	0.0000	0.0655	0.0000	0.0000
0.0000	0.0229	0.0000	0.0000	0.0000	0.0000	0.0545	−0.0263
0.0000	−0.0009	0.0000	0.0000	0.0000	0.0000	−0.0263	0.0266

Table 14: Partial squared length of the first 8 numerical mode shapes estimated with equation (32). Wood Part.

Numerical wood							
0.0703	0.0000	0.0000	−0.0136	0.0000	0.0138	0.0000	0.0000
0.0000	0.0665	0.0000	0.0000	0.0000	0.0000	−0.0261	−0.0009
0.0000	0.0000	0.0874	0.0000	0.0000	0.0000	0.0000	0.0000
−0.0136	0.0000	0.0000	0.0737	0.0000	0.0242	0.0000	0.0000
0.0000	0.0000	0.0000	0.0000	0.0878	0.0000	0.0000	0.0000
0.0138	0.0000	0.0000	0.0242	0.0000	0.0145	0.0000	0.0000
0.0000	−0.0261	0.0000	0.0000	0.0000	0.0000	0.0269	0.0289
0.0000	−0.0009	0.0000	0.0000	0.0000	0.0000	0.0289	0.0568

Table 15: Total squared length of the first 8 numerical mode shapes estimated with equation (32).

Numerical total							
0.0619	0.0000	0.0000	−0.0100	0.0000	0.0098	0.0000	0.0000
0.0000	0.0591	0.0000	0.0000	0.0000	0.0000	−0.0189	−0.0011
0.0000	0.0000	0.0746	0.0000	0.0000	0.0000	0.0000	0.0000
−0.0100	0.0000	0.0000	0.0647	0.0000	0.0173	0.0000	0.0000
0.0000	0.0000	0.0000	0.0000	0.0749	0.0000	0.0000	0.0000
0.0098	0.0000	0.0000	0.0173	0.0000	0.0221	0.0000	0.0000
0.0000	−0.0189	0.0000	0.0000	0.0000	0.0000	0.0311	0.0206
0.0000	−0.0011	0.0000	0.0000	0.0000	0.0000	0.0206	0.0522

Table 16: Partial squared length of the first 8 experimental mode shapes estimated with equation (35). Steel Part.

Experimental steel							
0.2914	0.0023	0.0001	−0.1089	0.0030	0.1938	0.0047	0.0031
0.0023	0.2701	0.0009	−0.0002	0.0004	0.0095	0.2765	0.0111
0.0001	0.0009	0.0005	−0.0001	0.0000	0.0004	0.0011	0.0001
−0.1089	−0.0002	−0.0001	0.0477	−0.0014	−0.1222	−0.0006	−0.0012
0.0030	0.0004	0.0000	−0.0014	0.0001	0.0045	−0.0014	−0.0011
0.1938	0.0095	0.0004	−0.1222	0.0045	0.5860	0.0132	0.0065
0.0047	0.2765	0.0011	−0.0006	−0.0014	0.0132	0.5168	0.1664
0.0031	0.0111	0.0001	−0.0012	−0.0011	0.0065	0.1664	0.1037

Table 17: Partial squared length of the first 8 experimental mode shapes estimated with equation (35). Wood Part.

Experimental wood							
1.3282	−0.0026	−0.0141	0.1143	−0.0028	−0.1569	0.0003	0.0075
−0.0026	1.0167	0.0058	0.0116	−0.0137	0.0039	−0.2695	0.0145
−0.0141	0.0058	0.3302	−0.0076	0.0085	−0.0045	−0.0040	0.0034
0.1143	0.0116	−0.0076	0.3317	−0.0022	0.1146	−0.0092	0.0018
−0.0028	−0.0137	0.0085	−0.0022	0.2219	−0.0055	0.0055	−0.0049
−0.1569	0.0039	−0.0045	0.1146	−0.0055	0.0741	−0.0033	0.0009
0.0003	−0.2695	−0.0040	−0.0092	0.0055	−0.0033	0.1779	−0.1420
0.0075	0.0145	0.0034	0.0018	−0.0049	0.0009	−0.1420	0.2219

Table 18: Total squared length of the first 8 experimental mode shapes estimated with equation (35).

Experimental total							
1.1736	−0.0018	−0.0120	0.0818	−0.0020	−0.1040	0.0009	0.0069
−0.0018	0.9048	0.0051	0.0099	−0.0116	0.0047	−0.1890	0.0155
−0.0120	0.0051	0.2818	−0.0065	0.0073	−0.0038	−0.0032	0.0030
0.0818	0.0099	−0.0065	0.2900	−0.0021	0.0793	−0.0079	0.0014
−0.0020	−0.0116	0.0073	−0.0021	0.1893	−0.0040	0.0045	−0.0043
−0.1040	0.0047	−0.0038	0.0793	−0.0040	0.1511	−0.0008	0.0017
0.0009	−0.1890	−0.0032	−0.0079	0.0045	−0.0008	0.2293	−0.0959
0.0069	0.0155	0.0030	0.0014	−0.0043	0.0017	−0.0959	0.2041

Table 19: Numerical $\mathbf{M_{FEs}}/\mathbf{M_{FEw}}$ and experimental $\mathbf{M_{Xs}}/\mathbf{M_{xw}}$ ratios.

Numerical $\mathbf{M_{FEs}}/\mathbf{M_{FEw}}$		Error (%)	Experimental $\mathbf{M_{Xs}}/\mathbf{M_{xw}}$		Error (%)
Exact	Equation (27)		Exact	Equation (27)	
1.1361	1.128	2.2	1.0436	0.9199	11.85

Table 20: Masses M_{Xs} and M_{Xw} estimated with equation (56).

	Exact	Modal masses (data from Table 10) used in the calculations		
		$\mathbf{m_{FE}}$	$\mathbf{m_{X2}}$	$\mathbf{m_{X3}}$
$\mathbf{M_{Xs}}$ (kg)	11.96	13.7754	12.6894	12.7804
$\mathbf{M_{Xw}}$ (kg)	11.46	11.6517	11.6893	10.6948
$\mathbf{M_{Xs}}/\mathbf{M_{Xw}}$	1.0436	1.1823	1.0856	1.1950
Residual error		0.0328	0.0056	0.0710

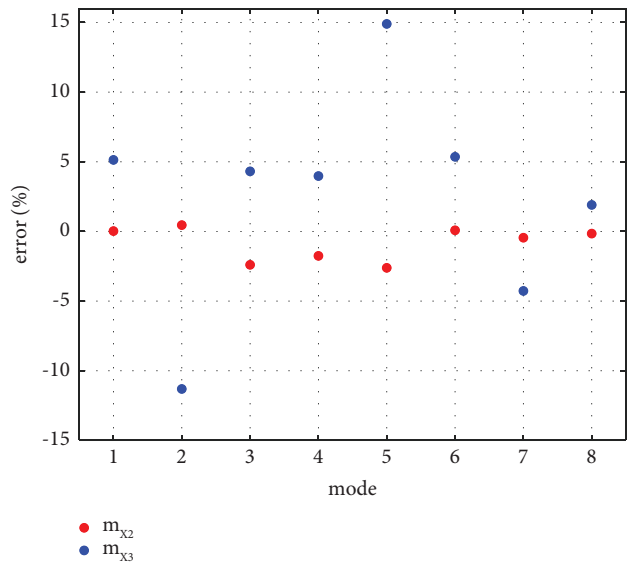

Figure 9: Errors between the modal masses obtained with the least square solutions and the modal masses m_{X2} and m_{X3}.

7. Conclusions

The present study provides a comprehensive explanation of the concept of cross-length of mode shapes. Firstly, the cross-length of a continuous mode shape is defined, which is then extended to discrete systems, introducing the concept of a length matrix. Furthermore, an approach for calculating the length and the cross-length of experimental mode shapes has been developed utilizing the structural dynamic modification theory, where the experimental model is considered a perturbation of the numerical model.

It is demonstrated that the cross-length between mode shapes must be zero in constant mass density systems. Due to the fact that the modal masses of the different modes are related by (37) in constant mass density systems, a proportional frequency response function (FRF) and a proportional change flexibility matrix can be constructed in these systems even though the modal masses are not known.

If the structure is constituted by two parts with different mass densities, it is demonstrated that the ratio of the partial cross-lengths over the two volumes is constant for all the modes and equal to the ratio of the total masses of such volumes. This information can be used to know how the mass is distributed in the structure. If the modal masses are known, the mass distribution can also be obtained using the partial lengths over the two volumes.

In order to validate the equations proposed in this paper and study their accuracy, two lab-scaled structures were constructed. The first one, an *L*-shape lab-scaled steel structure, has constant mass density, whereas the second one, a T-shape lab-scaled structure, consists of two different materials, with the column made of steel and the beam made of wood. Finite element models were also assembled in ABAQUS for both structures. The finite element models were intentionally not updated in order to check the effectiveness of the proposed methodology in cases where there is not a perfect numerical-experimental correlation. The modal masses were obtained from the FE models, estimated with experimental modal analysis and combined with the numerical and experimental mode shapes.

For the L-shape structure, although there are significant discrepancies between the numerical and experimental models, the squared length L_X^2 has been estimated with good accuracy (35). This demonstrates that the methodology proposed in Section 4 can be successfully utilized to determine the length of experimental mode shapes. It was also proved that the ratio modal mass-squared length of the mode shapes is constant for all the modes and equal to the total mass of the system in constant mass density systems. This information can be utilized to check if the experimental modal masses have been estimated accurately.

For the T-shape structure, the concept of cross-length was used to determine how the mass is distributed in the structure. Despite significant discrepancies between the numerical and experimental models (discrepancies in natural frequencies up to 35%), the ratio of the masses of the steel and the wooden parts was estimated with an error of less than 12%. The modal masses and the length of the mode shapes were also used to estimate the total masses of the steel and wooden parts with equation (56), with errors depending on the accuracy of the experimental modal masses. The total masses of the steel and wooden parts were used to determine if some of the modal masses were not estimated accurately.

Data Availability

Model properties and natural frequencies used to support the findings of this study are included within the article. The mode shape data are available from the corresponding author upon request.

Conflicts of Interest

The authors declare that they have no conflicts of interest.

Acknowledgments

The authors would like to express their gratitude to the Spanish Ministry of Science and Innovation for the financial support through the project MCI-20-PID2019-105593GB-I00/AEI/10.13039/501100011033.

References

[1] A. Brandt, M. Berardengo, S. Manzoni, and A. Cigada, "Scaling of mode shapes from operational modal analysis using harmonic forces," *Journal of Sound and Vibration*, vol. 407, pp. 128–143, 2017.

[2] D. Bernal, "A receptance based formulation for modal scaling using mass perturbations," *Mechanical Systems and Signal Processing*, vol. 25, no. 2, pp. 621–629, 2011.

[3] G. Coppotelli, "On the estimate of the FRFs from operational data," *Mechanical Systems and Signal Processing*, vol. 23, no. 2, pp. 288–299, 2009.

[4] M. M. Khatibi, M. R. Ashory, A. Malekjafarian, and R. Brincker, "Mass–stiffness change method for scaling of operational mode shapes," *Mechanical Systems and Signal Processing*, vol. 26, pp. 34–59, 2012.

[5] M. López-Aenlle, P. Fernández, R. Brincker, and A. Fernández-Canteli, "Scaling-factor estimation using an optimized mass-change strategy," *Mechanical Systems and Signal Processing*, vol. 24, no. 5, pp. 1260–1273, 2010.

[6] Y. Tian, J. Zhang, and Y. Han, "Structural scaling factor identification from output-only data by a moving mass technique," *Mechanical Systems and Signal Processing*, vol. 115, pp. 45–59, 2019.

[7] Y. Tian, L. Wang, and J. Zhang, "Time-varying frequency-based scaled flexibility identification of a posttensioned concrete bridge through vehicle–bridge interaction analysis," *Structural Control and Health Monitoring*, vol. 28, no. 1, 2021.

[8] Y. Tian and J. Zhang, "Structural flexibility identification via moving-vehicle-inducedtime-varying modal parameters," *Journal of Sound and Vibration*, vol. 474, Article ID 115264, 2020.

[9] B. Cauberghe, P. Guillaume, P. Verboven, and E. Parloo, "Identification of modal parameters including unmeasured forces and transient effects," *Journal of Sound and Vibration*, vol. 265, no. 3, pp. 609–625, 2003.

[10] W.-Y. He, W.-X. Ren, and X.-H. Zuo, "Mass-normalized mode shape identification method for bridge structures using parking vehicle-induced frequency change," *Structural*

Control and Health Monitoring, vol. 25, no. 6, Article ID e2174, 2018.

[11] M. Sheibani, A. H. Hadjian-Shahri, and A. K. Ghorbani-Tanha, "Mass scaling of mode shapes based on the effect of traffic on bridges: a numerical study," *Dynamics of Civil Structures*, vol. 2, pp. 95–106, 2017.

[12] M. Sheibani and A. K. Ghorbani-Tanha, "Obtaining mass normalized mode shapes of motorway bridges based on the effect of traffic movement," *Structures*, vol. 33, pp. 2253–2263, 2021.

[13] E. Reynders, D. Degrauwe, G. De Roeck, F. Magalhães, and E. Caetano, "Combined experimental-operational modal testing of footbridges," *Journal of Engineering Mechanics*, vol. 136, no. 6, pp. 687–696, 2010.

[14] J. Cara, "Computing the modal mass from the state space model in combined experimental–operational modal analysis," *Journal of Sound and Vibration*, vol. 370, pp. 94–110, 2016.

[15] P. Guillaume, T. De Troyer, C. Devriendt, and G. De Sitter, "Omax - a combined experimental-operational modal analysis approach," *Proc. ISMA2006 Int. Conf. Noise Vib. Eng.*, 2006.

[16] J.-S. Hwang, H. Kim, and J. Kim, "Estimation of the modal mass of a structure with a tuned-mass damper using H-infinity optimal model reduction," *Engineering Structures*, vol. 28, no. 1, pp. 34–42, 2006.

[17] J. M. W. Brownjohn and A. Pavic, "Experimental methods for estimating modal mass in footbridges using human-induced dynamic excitation," *Engineering Structures*, vol. 29, no. 11, pp. 2833–2843, 2007.

[18] A. Brandt, M. Berardengo, S. Manzoni, M. Vanali, and A. Cigada, "Global scaling of operational modal analysis modes with the OMAH method," *Mechanical Systems and Signal Processing*, vol. 117, pp. 52–64, 2019.

[19] O. Abdeljaber, M. Dorn, and A. Brandt, "Scaling an oma modal model of a wood building using omah and a small shaker," *Topics in Modal Analysis \& Testing*, vol. 8, pp. 151–157, 2021.

[20] A. Brandt, M. Berardengo, S. Manzoni, M. Vanali, and A. Cigada, "Overview of the new OMAH technique for scaling OMA mode Shapes戔," *Sound and Vibration*, vol. 52, no. 3, pp. 1–5, 2018.

[21] M. L. Aenlle and R. Brincker, "Modal scaling in operational modal analysis using a finite element model," *International Journal of Mechanical Sciences*, vol. 76, pp. 86–101, 2013.

[22] D. J. Ewins, *Modal Testing: Theory, Practice and Application*, Wiley, Hoboken, NJ, USA, 2000.

[23] N. Mendes Maia and J. Montalvão Silva, *Theoretical and Experimental Modal Analysis*, Research Studies Press, Boston, Massachusetts, UK, 1997.

[24] W. Heylen, S. Lammens, and P. Sas, *Modal Analysis Theory and Testing*, Katholieke Universiteit Leuven, Belgium, Europe, 2007.

[25] R. Brincker and C. E. Ventura, *Introduction to Operational Modal Analysis*, John Wiley & Sons, Ltd, Chichester, UK, 2015.

[26] R. W. Clough and J. Penzien, *Dynamics of Structures*, McGraw-Hill, New York, NY, USA, 1993.

[27] A. K. Chopra, *Dynamics of Structures*, Prentice Hall, New Jersey, NJ, USA, 1995.

[28] M. Paz and Y. H. Kim, *Structural Dynamics: Theory and Computation*, Kluwer Academic Publishers, Boston, Massachusetts, UK, 1993.

[29] M. Aenlle, M. Juul, and R. Brincker, "Modal mass and length of mode shapes in structural dynamics," *Shock and Vibration*, vol. 2020, Article ID 8648769, 16 pages, 2020.

[30] M. Aenlle, M. Juul, and R. Brincker, "Corrigendum to "modal mass and length of mode shapes in structural dynamics," *Shock and Vibration*, vol. 2021, Article ID 9821852, 16 pages, 2021.

[31] M. López-Aenlle, R. Brincker, F. Pelayo, and A. F. Canteli, "On exact and approximated formulations for scaling-mode shapes in operational modal analysis by mass and stiffness change," *Journal of Sound and Vibration*, vol. 331, no. 3, pp. 622–637, 2012.

[32] S. A. Dianat and E. Saber, *Advanced Linear Algebra for Engineers with MATLAB*, CRC Press, New York, NY, USA, 2009.

[33] D. J. Ewins, "Model validation: correlation for updating," *Sadhana*, vol. 25, no. 3, pp. 221–234, 2000.

[34] R. J. Allemang and D. Brown, "Correlation coefficient for modal vector analysis," in *Proceedings of the 1st International Modal Analysis Conference. Orlando: International Society for Optical Engineering and Society for Experimental Mechanics*, pp. 110–116, Orlando, FL, USA, November 1982.

[35] R. J. Allemang, "The modal assurance criterion - twenty years of use and abuse," *Sound and Vibration*, vol. 37, 2003.

[36] S. S. Rao, *Vibration of Continuous Systems*, John Wiley & Sons, New Jersey, NJ, USA, 2007.

[37] A. W. Leissa and M. S. Qatu, *Vibrations of Continuous Systems*, McGraw-Hill, New York, NY, USA, 2011.

[38] A. Sestieri and W. D'Ambrogio, "A modification method for vibration control of structures," *Mechanical Systems and Signal Processing*, vol. 3, pp. 229–253, 1989.

[39] A. Sestieri, "Structural dynamic modification," *Sadhana - Acad Proc Eng Sci*, vol. 25, 2000.

[40] P. Avitabile, "Twenty years of structural dynamic modification - a review," *SV: Sound & Vibration*, vol. 37, 2003.

[41] D. S. S. Corp, *Abaqus User's Manual*, Rhode Island, Providence, USA, 2020.

[42] N. Instruments, *LabVIEW User Manual*, National Instruments Corp, Austin, Texas, USA, 2003.